Dense-Phase Feeding of Pulverized Coal in Uniform Plug Flow

A series of high-pressure pneumatic dense-phase flow experiments were conducted using pulverized coal as the granular solids. This granular material was transported by nitrogen gas out of a conical feeder tank, through a length of stainless-steel tubing and into a pressurized receiver tank. Only the nitrogen gas trapped in the interstices of the coal particles inside the feeder tank was used to transport the coal. Six different transport stainless-steel tube geometries were used. A detailed analysis of the system is performed. This analysis reasonably predicts the expected solids flow rate for a given set of operating conditions and the minimum pressure drop required to maintain flow.

K. M. SPROUSE and M. D. SCHUMAN

Energy Systems Group
Rockwell International
Canoga Park, CA 91304

SCOPE

Pneumatic conveying of pulverized solids is an extremely interesting field of study. Many different types of transport systems have been developed for commercial use as described by Kraus (1980). Perhaps the most reliable technique for conveying bulk materials is the dilute-phase transport method which mechanically feeds granular solids into a high-velocity gas stream. This highly turbulent gas stream rapidly entrains the particles and prevents them from settling out as the solids are transported over a given distance.

Dilute-phase transport is characterized to a great degree by extremely high gas to solids volume conveying ratios and low gas pressure drops. For many applications, these high volume ratios are not desirable due to restrictions on feed system size, gas compressor or blower power requirements, or the amount of carrier gas allowed for conveying. In response to these restrictions, commercial systems are now available which significantly reduce the gas to solids volume ratio. The trade-off that occurs by reducing the transport volume ratio is that the gas pressure drop across the feed line is significantly raised, and since the solid particles are in much closer contact with one another, the chances of plugging the feed line are greatly increased.

Wen and O'Brien (1976) and Klinzing (1981) have reviewed the types of analyses and experimental studies which have been used in designing both dilute-phase transport systems and those using lower gas to solids volume ratios. They have indicated that by lowering the volume ratio, a flow condition will be reached whereby the solids will begin to separate out from the main gas stream and flow in a nonuniform condition. This flow regime has been defined as dense-phase solids transport. However, once the volume ratio has been reduced to the point where the entire transport line is filled with granular material at or near its static bed void fraction, Wen and O'Brien (1976) and Klinzing (1981) indicate that the pipe will plug, thus terminating flow.

Experimental efforts by Burge et al. (1964), Sandy et al. (1970), Oberg et al. (1977, 1982), and Friedman (1979) have shown that this is not necessarily true with proper feed system design. Reliable dense-phase feeding in uniform plug flow can be maintained by keeping inside pipe walls smooth with no sudden cross-sectional area contractions or expansions and by providing sufficient gas pressure drop through the feed system.

The objectives of this study were to begin with the development of an adequate dense-phase flow data base for these extremely low gas to solids volume ratios and to begin the development of an accurate two-phase flow model which will predict the experimental results. For this study, a high-pressure test facility was selected to minimize the gas-phase volume expansion through the transport line due to pressure drop. By minimizing the gas-phase volume expansion, the solids are assured to move through the entire test line at or near their static bed void fraction in uniform dense-phase plug flow.

CONCLUSIONS AND SIGNIFICANCE

A series of experiments were conducted over a wide range of operating conditions to aid in the development of a detailed dense-phase flow model. These experiments were conducted at high pressure (greater than 7 MPa) in transport lines of six different geometries. The results show the effect of system pressure drop with solids flow rate, including the minimum pressure drop allowable for maintaining solids flow.

A mathematical model was developed from first principles and was found to reasonably predict the experimental results. This model should be capable of predicting the solids flow rate for feed system geometries other than those tested here. However, the bulk material properties of each granular solids to be conveyed must be determined beforehand.

This study should greatly aid the commercial development of this new ultra-dense-phase feeding method. Conveying pulverized material pneumatically at its static bed void fraction significantly reduces the amount of carrier gas required for transporting. For many applications this reduced transport gas requirement can be economically attractive. Feed systems can be made more compact and power requirements for gas compression lowered.

BACKGROUND

The pneumatic conveying of granular solids can be achieved over a wide range of operating conditions. Wen and O'Brien (1976) and Klinzing (1981), for example, have described many of the diverse characteristics and flow parameters associated with this type of solids conveying. Basically, these authors indicate that pneumatic transport of granular materials can occur by one of three flow regimes, Figure 1. These classifications are the dilute-phase transport regime, the dense-phase transport with nonuniform flow regime,

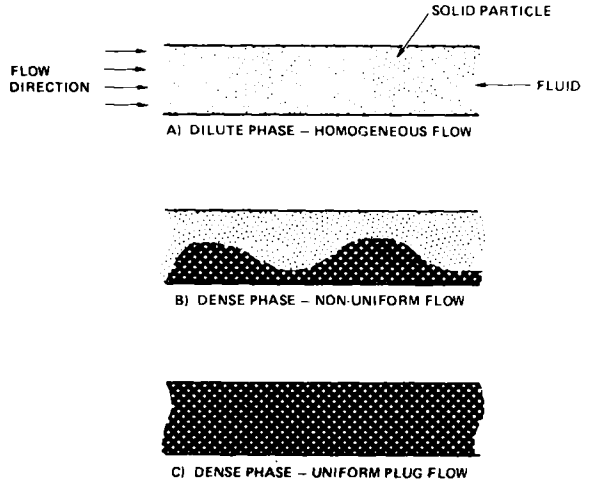

Figure 1. Flow regimes of fluid-solids two-phase transport in a horizontal tube.

and the dense-phase transport with uniform plug-flow regime. The major distinguishing flow characteristics among these three methods of solids feeding are that higher solids-gas ratios, transport line pressure gradients, and solids mass fluxes will be produced as the conveying system is changed from dilute-phase to uniform plug-flow dense-phase feeding.

Dilute-phase transport, Figure 1A, occurs whenever the solid granules are homogeneously dispersed throughout the transport line and the void fraction, ϵ, of the gas-solids mixture inside the line is very high, usually greater than 0.90. To maintain this condition, the gas velocity inside the transport line is kept well into the turbulent regime so that turbulent fluctuations will offset the gravitational effects, thus keeping the solids well dispersed.

However, when the gas velocity falls below the saltation velocity in horizontal flow or the choking velocity in rising vertical flow, the granular solids will begin to settle out and flow nonuniformly inside the transport line. The saltation and choking velocities are complex functions of the gas and solid densities, the gas viscosity, the pipe and particle diameters, and the gas-solids void fraction. However, Wen and O'Brien (1976) and Klinzing (1981) provide a number of correlations for determining these two important limiting velocities.

Once the gas velocity has fallen below the saltation or choking velocity, the bulk of the granular solids will be flowing through the transport line at or very near their static bed void fraction separated from the bulk of the transport gas. This condition, Figure 1B, has been classified as dense-phase, nonuniform flow since the bulk of the solid material is in fact being transported in a very dense condition. The types of flow patterns associated with nonuniform dense-phase feeding are quite varied. Wen and O'Brien (1976), for example, have shown at least eight distinguishable flow patterns for the regime described by Figure 1B and have indicated that these flows are usually quite unstable, producing large fluctuations in both solids flow rate and transport line pressure drop.

Uniform plug-flow dense-phase feeding, Figure 1C, is achieved by continuing to increase the solids-gas ratio until the entire transport line is filled with granular solids at or near their static bed void fraction. At this condition, the entire granular mass will be moving at near constant velocity everywhere inside the transport line with little, if any, particle velocity gradients in the radial direction of the tube. Considerable care must be given to the design and operation of this type of flow system, since it is extremely easy for the solid granules to bridge or arch across the transport line, thus stopping the entire solids-gas flow. Wen and O'Brien (1976) have classified this flow pattern as the "pipe-plugged" regime, no doubt in response to this arching problem. However, if the transport lines are kept relatively smooth with no sudden cross-sectional area contractions or expansions, reliable dense-phase solids feeding can be maintained. Unlike nonuniform dense-phase flow, Oberg et al. (1982) have shown this type of solids feeding to be very steady with little, if any, solids flow rate or transport line pressure drop oscillations.

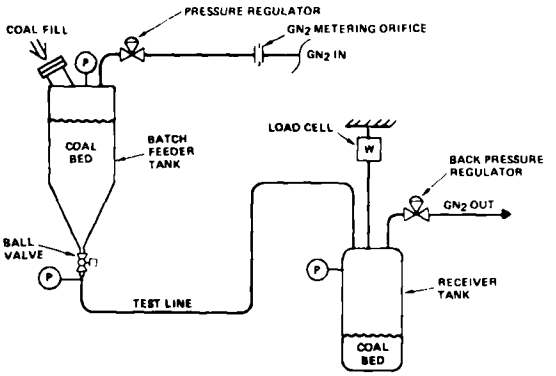

Figure 2. Dense-phase feed system and test facility schematic for uniform plug flow.

Most of the commercial pneumatic conveying systems and related equipment used in solids transport have been described by Kraus (1980). To date, these commercial conveying systems have only addressed dilute-phase transport and nonuniform-flow dense-phase feeding. Dilute-phase conveying systems generally employ rotary airlock feeders or screw feeders to mechanically convey the granular solids out a storage bin and into the pneumatic transport line where these solid particles are rapidly mixed with transport gas supplied by blowers. Fluidized-bed (blow tank) feeders are used primarily for producing nonuniform-flow dense-phase transport.

Although not yet commercialized, uniform plug-flow dense-phase feed systems are much simpler in design than their dilute-phase and nonuniform dense-phase counterparts. A schematic representation of the basic plug-flow dense-phase feed system is shown in Figure 2. The system consists of a feeder tank which is fed by a regulated compressed gas supply at its upper end while the lower portion of the tank is connected to the solids transport line. A ball valve located at the exit of the feeder tank remains closed until the feeder tank has been pressurized to design flow conditions. The feeder tank's discharge cone is sized for an included angle in the range of 20–40 degrees so that good solids mass flow inside the feeder tank is achieved without rat holing. Coal is loaded intermittently through a coal fill port at the top of the feeder vessel, and the system is operated in the batch mode.

Initial studies in dense-phase solids transport, using a feeder method similar to that described in Figure 2, have been conducted by Burge et al. (1964) and Sandy et al. (1970). These studies established the feasibility of dense-phase solids transport with this type of feeder method. However, in both studies, the transport line discharge pressure was kept at 1 atm, thereby producing a significant expansion of the transport gas inside the feed line. It is highly unlikely these researchers had uniform plug flow throughout their entire feed system. Once significant transport gas expansion has occurred, the flow will digress into either the nonuniform dense-phase or dilute-phase regime.

More recently, Oberg and Hood (1980) have made significant improvements in the dense-phase feed systems initially employed by Burge et al. (1964) and Sandy et al. (1970). This feeder method was first checked out with pulverized coal at atmospheric discharge pressures (Oberg et al., 1977). However, later efforts have shown successful operation to discharge pressures in excess of 10 MPa (100 atm) (Friedman, 1979; Oberg et al., 1982). At these extremely high discharge pressures, the carrier gas is essentially incompressible; therefore, dense-phase feeding with uniform plug flow will be maintained throughout the entire transport line.

The dense-phase feeder method, Figure 2, is not limited only to intermittent or batch-mode operation. Further testing has shown this method to be capable of continuous steady-state operation whenever a pair of cycling lock hoppers are plumbed into the upper end of the dense-phase feeder tank. By maintaining constant feeder tank gas pressure and sufficient transport line pressure drop,

the bed height of the granular solids can either rise or fall inside the tank without causing any significant variations in the solids discharge flow rate. A continuous high-pressure dense-phase feed system using this method for coal gasification processes is given by Combs et al. (1980).

GENERAL THEORY OF FLUID-SOLIDS TRANSPORT

Wen and O'Brien (1976) and Klinzing (1981) have provided some analytical methods for studying gas-solids transport. However, none of these methods address uniform plug-flow dense-phase feeding. Instead of attempting to extrapolate the semi-empirical results given for nonuniform-flow dense-phase transport to the plug-flow regime, an analysis based on first principles will be developed for isothermal transport. This analysis follows a continuum rather than a kinetic theory approach and is predicated on laminar flow arguments. Although the main thrust of this general theory is to provide the governing equations for plug-flow dense-phase transport, it is expected these equations will also govern a wide variety of two-phase flow conditions. Anticipated applications of this theory include particle-gas separation in cyclones, gravity flow of granular materials out of bins and hoppers, and soil mechanic analyses.

Most of the following equations are written in vector short-hand notation where ∇ is the vector differential operator, $\bar{\bar{\delta}}$ is the unit tensor, D/Dt is the total time or substantial derivative, ∂ is the partial derivative, and superscript T denotes the transpose of a tensor. An excellent summary of vector notation is given by Bird et al. (1960).

Continuity

For fluid-solids flow which can be characterized as a continuum, a fluid mass conservation analysis will show:

$$\frac{\partial(\epsilon\rho_f)}{\partial t} + \nabla\cdot(\epsilon\rho_f\vec{v}_f) = 0 \tag{1}$$

For the granular material, a solids mass balance yields

$$\frac{\partial[(1-\epsilon)\rho_s]}{\partial t} + \nabla\cdot[(1-\epsilon)\rho_s\vec{v}_s] = 0 \tag{2}$$

In Eqs. 1 and 2, the fluid velocity, $\vec{v}_f$, is not necessarily equal to the solids velocity, $\vec{v}_s$.

Momentum

The two equations of momentum for the fluid and solids respectively are:

$$\epsilon\rho_f\frac{D\vec{v}_f}{Dt} = -\nabla\cdot(\epsilon\vec{\tau}_f) + \epsilon\rho_f\vec{g} - \vec{B} \tag{3}$$

and

$$(1-\epsilon)\rho_s\frac{D\vec{v}_s}{Dt} = -\nabla\cdot[(1-\epsilon)(\vec{\tau}_f + \vec{\tau}_s)] + (1-\epsilon)\rho_s\vec{g} + \vec{B} \tag{4}$$

Equations 3 and 4 simply state that material acceleration within the control volume is equal to the sum of the surface forces acting on the material plus the gravitational force and fluid-solids drag body force, $\vec{B}$.

The fluid stress tensor, $\vec{\tau}_f$, and solids stress tensor, $\vec{\tau}_s$, are based on unit fluid and solid areas, respectively. Equations 3 and 4 show that, for these surface forces, the control volume surface area occupied by the fluid is equal to the void fraction, ϵ. (This is easily determined from continuity relationships.) However, this is only true within the bulk flow stream. At physical boundaries (e.g., a pipe wall), the solid granules will not penetrate this surface as they can the imaginary surfaces of a control volume. Therefore, the void surface area fraction does not equal ϵ at these locations, but instead will always be very close to 1.0.

The solids stress tensor, $\vec{\tau}_s$, is defined as only those stresses which can be transmitted through particle-particle contact, such as through frictional sliding and particle collision. However, since the carrier fluid uniformly surrounds each particle, the actual stresses carried through the granular medium are those due to the sum of both fluid and solids stress tensors and not simply those contributed by the solids stress tensor alone. By defining $\vec{\tau}_s$ in this fashion, bouyancy effects due to the differences in fluid and solid particle densities can be more easily shown. Eliminating $\vec{\tau}_f$ from Eqs. 3 and 4, through substitution, will give the proper mathematical relation.

Fluid-Solids Drag Body Force Vector ($\vec{B}$)

The fluid-solids drag body force vector is a strong function of the flow void fraction. It is well known that as ϵ approaches 1.0, the laminar drag force vector will approach the classical Stokes flow law (Bird et al., 1960). This condition is given by:

$$\vec{B} = \frac{18(1-\epsilon)\mu(\vec{v}_f - \vec{v}_s)}{D_p^2} \tag{5}$$

However, it is also known that when the void fraction drops below 0.5, the laminar drag body force vector is replaced by the Blake-Kozeny equation (Bird et al., 1960). This equation is:

$$\vec{B} = \frac{150(1-\epsilon)^2\mu(\vec{v}_f - \vec{v}_s)}{\epsilon^2 D_p^2} \tag{6}$$

Expressions for the laminar drag body force vector have not been reported in the literature for void fractions between 0.5 and 1.0. When ϵ is in this range, the drag force is usually assigned to either Eq. 5 or 6 depending on how close ϵ is to these two limiting values.

Equations 5 and 6 should be used only when the Reynolds number, based on fluid flow past a particle is in the laminar regime (less than approximately 1.0). For particles, with diameters under 100 μm, this is generally the case for most conditions.

When considering granular materials composed of particles having multiple diameters, Eqs. 5 and 6 must be control-volume-averaged over the entire particle size number distribution, f_n. Assuming the void fraction, ϵ, is independent of the particle size, it can be shown that the particle diameter, D_p, in Eqs. 5 and 6 is equal to the volume-diameter mean, D_{31}, where:

$$D_{31} = \left[\frac{\int_0^\infty D_p^3 f_n dD_p}{\int_0^\infty D_p f_n dD_p}\right]^{1/2} \tag{7}$$

Fluid Stress Tensor ($\vec{\tau}_f$)

For Newtonian fluids, it is well known that as ϵ approaches 1.0, the fluid stress tensor for laminar flow is equal to:

$$\vec{\tau}_f = \left[P_f + \left(\frac{2}{3}\mu - \kappa\right)\nabla\cdot\vec{v}_f\right]\bar{\bar{\delta}} - \mu\left[(\nabla\vec{v}_f) + (\nabla\vec{v}_f)^T\right] \tag{8}$$

The validity of this equation has yet to be determined for void fractions well below 1.0 and in these regimes Eq. 8 should be used with caution.

Solids Stress Tensor ($\vec{\tau}_s$)

Perhaps the most unsettled of all relations concerning dense-phase solids transport is the solids stress tensor, $\vec{\tau}_s$. Most researchers have proposed numerous constitutive relations for this tensor, often in direct conflict with the work of others. A complete discussion of the theoretical and experimental aspects surrounding the quantification of this tensor would fill a volume much larger than contemplated here. A brief review of these previous studies is given in the Supplementary Material Section. (The supplementary ma-

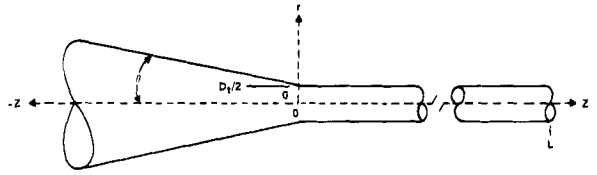

Figure 3. Transport test line and converging hopper geometry.

terial section of this paper can be obtained in microfilm or hard copy by writing *AIChE Journal.*)

UNIFORM DENSE-PHASE FLOW IN A TUBE

Consider a tube of diameter D_t and length L as shown in Figure 3. A cylindrical coordinate system is placed on this tube such that its origin is located at the tube's entrance, and fluid flow is in the positive z-direction. The granular solids are closely packed so that fluid-solids transport is in the uniform plug-flow dense-phase regime. In developing the equations governing the dense-phase flow of granular materials in this tube, the following assumptions are used.

(A) The fluid and solids flows are one-dimensional, steady state in the z-direction.

(B) The fluid is incompressible; ρ_f is constant.

(C) The solid particles are also incompressible; ρ_s is constant.

(D) The fluid stress tensor, $\bar{\tau}_f$, is given by Eq. 8 with the fluid bulk viscosity, κ, equal to zero.

(E) Compressive stresses of the solids stress tensor, $\bar{\tau}_s$, are only those due to solids static pressure, P_s.

(F) Fluid pressure, P_f, and solids pressure, P_s, are constant in the r-direction.

(G) All tangential gradients are negligible.

(H) Body forces due to gravity are negligible.

(I) The void fraction, ϵ, is constant over the entire flow.

(J) The fluid-solids drag body force vector, $\vec{B}$, is given by Eq. 6 (the Blake-Kozeny equation).

(K) Gradients of solids velocity are negligible in the r-direction; the granular material flows as a uniform plug.

(L) The ratio of tube diameter, D_t, to particle diameter, D_p, is very large.

(M) The ratio of tube length, L, to tube diameter, D_t, is also very large.

(N) The ratio of the solids surface area fraction at the tube wall to that in the bulk is extremely small; that is, $\alpha \ll 1.0$.

Assumptions A through H are straightforward and need no further explanation, except emphasizing that should the transport fluid be a gas rather than a liquid, assumption B requires the total line pressure drop to be much smaller than the absolute system pressure. The void fraction ϵ in assumption I is actually a function of a solids compressibility relation. However, this relation is not well known; since for uniform plug-flow dense-phase feeding the granular material flows at or near its static bed void fraction, the assumption that ϵ is constant is reasonable. More will be said about assumption I in the Results Section.

The Blake-Kozeny drag relation, Eq. 6, has been used successfully in predicting laminar flow pressure drops through packed beds where the bed void fraction is below 0.5. The static bed void fraction of a granular material can change quite dramatically over time depending on the level of compaction. It is well known that the minimum void fraction of a packed bed of uniform diameter spheres is given by tetrahedral-rectangular piling which leads to an ϵ of 0.260. However, loosely-packed static beds of granular materials can also have an ϵ even greater than 0.60. Thus, assumption J is most applicable for uniform plug-flow dense-phase feeding when the fluid flow past the particles is also in the laminar regime. For extremely small particles (under 100 μm) which are unrestrained in the direction of fluid flow, laminar flow will usually result.

Assumption K should be valid, when the entire solids flow is in the Coulomb friction regime (low ϵ everywhere) and the effective angle of friction between the solids and tube wall, δ_w, is less than the solids angle of internal friction, ϕ. For smooth stainless-steel tubes transporting pulverized coal, δ_w is on the order of 10–20 degrees (or less) while ϕ is in the range of 20–40 degrees. Assumption K effectively allows the governing solids momentum equation to be solved without requiring a definition of the solids stress tensor in regard to shearing stresses and strains.

Assumptions L and M require no explanation other than that they are reasonable for most dense-phase solids transport systems and greatly simplify the analytical solution. Finally, Assumption N is easily invoked after considering that ϵ at the tube wall approaches 1.0.

Using assumptions A through K, the equations of the general theory section can be simplified into two equations: one for fluid transport, and the other for solids. The fluid flow equation is given by:

$$\frac{dP_f}{dz} = \mu\left[\frac{d^2v_f}{dr^2} + \frac{1}{r}\frac{dv_f}{dr} - b(v_f - v_{s,t})\right] \tag{9}$$

and the solids flow equation is:

$$\frac{dP_s}{dz} = \frac{\mu b(v_f - v_{s,t})}{(1-\epsilon)} - \frac{d(r\tau_{s,rz})}{rdr} \tag{10}$$

where the fluid-solids drag constant, b, is given by:

$$b = \frac{150(1-\epsilon)^2}{\epsilon^3 D_p^2} \tag{11}$$

The boundary conditions required to solve Eqs. 9 and 10 are as follows.

At $z = 0$: $\quad P_f = P_{f,o}$ and $P_s = P_{s,o}$

At $z = L$: $\quad P_f = P_{f,L}$ and $P_s = 0$

At $r = 0$: $\quad \dfrac{dv_f}{dr} = 0$ and $\tau_{s,rz} = 0$

And at $r = D_t/2$: $\quad v_f = 0$ and $\tau_{s,rz} = (P_s + \alpha P_f)\sin\delta_w$

Solving Eq. 9 with its appropriate boundary conditions yields for the fluid velocity profile inside the tube:

$$v_f = \left[v_{s,t} + \frac{(P_{f,o} - P_{f,L})}{\mu b L}\right]\left[1 - \frac{I_o(r\sqrt{b})}{I_o\left(\dfrac{D_t\sqrt{b}}{2}\right)}\right] \tag{12}$$

where I_o is the modified Bessel function of the first kind, order zero. Equation 12 shows that the fluid velocity is largest at the tube centerline and goes to zero at the tube wall. Since the fluid density is constant (Assumption B), it is sometimes useful to define an area averaged fluid tube velocity that can be directly related to the fluid mass flow rate. This area averaged fluid velocity is defined as:

$$v_{f,t} = \frac{8}{D_t^2}\int_o^{D_t/2} r v_f dr \tag{13}$$

Substituting Eq. 12 into Eq. 13 and using Assumption L yields for the tube line pressure drop:

$$(P_{f,o} - P_{f,L}) = \mu b L(v_{f,t} - v_{s,t}) \tag{14}$$

Applying the appropriate boundary conditions to Eq. 10 while using Eq. 12 and Assumptions L, M, and N will provide another relation for the fluid line pressure drop. This equation is:

$$(P_{f,o} - P_{f,L}) = \frac{4L}{D_t}[C_{WF}(1-\epsilon)P_{f,L} + \mu\sqrt{b}v_{s,t}] \tag{15}$$

where the coefficient of tube wall friction is defined as:

$$C_{WF} = \alpha \sin\delta_w \tag{16}$$

It is interesting to see that the solids pressure, P_s, does not appear in Eq. 15. Assumption M is primarily responsible for this result.

Now consider a truncated cone with half angle θ and exit diameter D_t, Figure 3. A cylindrical coordinate system is placed on this cone such that its origin is located at the cone exit with the positive axial direction pointing away from the cone. The cone is considered to contain a granular material at or near its static bed void fraction and is pressurized on the inside by a fluid to a pressure of $P_{f,-\infty}$. At the discharge end of the cone, the fluid pressure has dropped to $P_{f,o}$. The following additional assumptions are introduced to aid in the solution technique.

(O) The fluid and solids flow inside the cone is one-dimensional, axisymmetric flow in the positive z-direction.

(P) The fluid stresses are only those due to hydrostatic pressure, P_f. Combining Assumptions O and P with the earlier assumptions of A through J will allow the fluid momentum equation (Eqs. 3 and 6) to be written as

$$\frac{\rho_f}{2C_D^2}\frac{dv_f^2}{dz} = -\frac{dP_f}{dz} - \mu b(v_f - v_s) \tag{17}$$

Since a converging cone is similar to a metering nozzle, a fluid discharge coefficient, C_D, has been added to Eq. 17 to account for the nonideal isentropic fluid flow. A similar equation could also be written for solids momentum; however, this equation is required only for determining the solids pressure at the cone exit. Since this latter momentum equation is not required for the determination of the solids flow rate, it will not be included in the following discussion.

The following boundary conditions are required to solve Eq. 17.

At $z = -\infty$: $P_f = P_{f,-\infty}$ and $v_f = 0$

And at $z = 0$: $P_f = P_{f,o}$ and $v_f = v_{f,t}$

The continuity relations (Eqs. 1 and 2) for steady-state, incompressible, axisymmetric flow can be used to show that the fluid-solids slip velocity anywhere in the cone is given by:

$$(v_f - v_s) = \frac{D_t^2(v_{f,t} - v_{s,t})}{(D_t - 2z\tan\theta)^2} \tag{18}$$

Combining Eqs. 17 and 18 and applying the appropriate boundary conditions will show that the integrated fluid momentum equation in the cone is:

$$\frac{\rho_f {v_{f,t}}^2}{2C_D^2} = (P_{f,-\infty} - P_{f,o}) - \frac{D_t\mu b(v_{f,t} - v_{s,t})}{2\tan\theta} \tag{19}$$

EXPERIMENTAL

A high-pressure test facility was constructed at Rockwell International for the quantification of uniform plug-flow dense-phase feed systems, Combs (1982). This facility is capable of feeding granular solids at pressures from atmospheric to greater than 12 MPa (120 atm) with a variety of transport gases. The main feeder tank has a capacity of 7,000 L while a number of receiver tanks are available with capacities up to 570 L.

Test Hardware and Coal/Transport Gas Specifications

A simplified schematic of the high-pressure test facility used for this study is shown in Figure 2. It consists of a feeder tank, test line, and receiver tank. The feeder and receiver tanks are maintained at constant gas pressure by pressure regulators during a run. The feeder tank also has a ball valve located at its discharge end for initiating and stopping the coal flow. This ball valve is large in relation to the transport line diameter so that an additional line reducer cone connects the ball valve to the transport line. Both the feeder tank and reducer cone were made with discharge cone half angles of 15 degrees. The feeder and receiver tanks are smooth carbon steel vessels while stainless steel was used for the various transport test lines.

Experimental testing was conducted in the batch-mode method of operation. In this method, the pulverized coal is first loaded into the main feeder tank in such fashion as to minimize its compaction. Once coal loading is complete, the feeder tank is slowly pressurized to the desired run condition so that any unnecessary further compaction of the coal bed is prevented. After this is completed, the entire feed system downstream of the feeder tank's ball valve is pressurized to the desired receiver tank run pressure. Finally the ball valve is opened and steady-state coal flow operation is initiated. The testing series is terminated once the feeder tank has been completely emptied or the receiver tank filled.

TABLE 1. COAL AND TRANSPORT GAS PROPERTIES

Coal—Kentucky #9 hvAb	
Proximate Analysis	
wt. % Moisture	2.55
wt. % Ash	8.92
wt. % Volatiles	36.67
wt. % Fixed Carbon	51.86
Higher Heating Value (kcal/g)	7.119
True Solids Density, ρ_s (g/cm^3)	1.395
Volume Diameter Mean of the Particle Size Number Distribution, D_{31} (μm)	28
Static Bed Void Fraction, ϵ (Relative Uncompacted State)	0.5714
Transport Gas—Nitrogen	
Temperature (°C)	21
Molecular Weight (g/mol)	28.0134
Viscosity, μ (centipoise)*	0.01891

* 1 centipoise = 1 mPa·s

The coal (i.e., solids) flow rate through the test line is metered by a load cell which measures the instantaneous change in the receiver tank weight. To determine the actual coal flow rate, this load cell measurement is corrected by the gas density in the receiver tank and the coal's true solids density. The proper mathematical relationship is found by performing a continuity balance on the receiver. The transport gas (i.e., fluid) flow rate is found by metering the flow rate of pressurizing gas into the feeder tank. A continuity balance on the feeder will give the proper equation for determining this experimental transport gas flow rate.

The pressure taps used for determining the gas density and pressure in the feeder and receiver tanks are located in the upper section of these vessels so that plugging by solid particles is prevented. A special pressure tap is also located at the entrance to the test line so that feed hopper and transport line pressure drops can be determined. This special tap is fabricated from a porous metal screen similar to that described by Klinzing (1981).

Table 1 shows the relevant properties of the coal and nitrogen transport gas used for these tests. The Kentucky #9 high volatile A bituminous (hvAb) coal properties were obtained from American Society for Testing and Materials (ASTM) procedures. The proximate analysis was determined from ASTM D 3172-73, the higher heating value from ASTM D 2015-77, the true solids density from ASTM D 167-73, the particle-size distribution from ASTM D 197-30, and the static bed void fraction from ASTM D 2854-70 and ASTM D 167-73. However, some of these coal analyses were modified to give the results in Table 1.

For example, in ASTM D 167-73, methanol was used as the displacing liquid instead of water, since methanol had been found to give results similar to nitrogen for other analyzed carbonaceous solids and nitrogen was to be used as the carrier fluid for these dense-phase flow experiments. In ASTM D 197-30, a 400 mesh screen (37 μm opening) was added to the procedure to achieve a more accurate assessment of the volume diameter mean, D_{31}, of the coal's particle size number distribution. The Kentucky #9 bituminous coal used in these experiments had been pulverized to a standard industrial grind, where over 90% of its total mass passed through a 200 mesh sieve (74 μm opening). By adding the 400 mesh screen, a reasonable log-probability equation could be fitted to the coal's particle-size mass distribution determined from ASTM D 197-30 methods. Following the analysis given by Mugele and Evans (1951), the D_{31} of the coal's particle-size number distribution was then determined.

The pulverized bituminous coal used in this study at 2.55 wt. % moisture is a relative cohesionless material. Therefore, the solids shearing stress, $\tau_{s,rz}$, at the transport tube wall (used in the solution of Eq. 10) was written without the cohesion term for Mohr-Coulomb friction. However, at coal moistures above approximately 20 wt. %, cohesion effects will become important, and any subsequent transport analysis must take them into account. Also, the static bed void fraction calculated from ASTM D 2854-70 and ASTM D 167-73 procedures represents a relative loosely-packed solids bed. The manner in which the coal feeder tank is filled and its solids bed fluffed between dense-phase flow experiments has been shown to produce a static bed void fraction quite similar to the ASTM D 2854-70 standard test method.

Transport Analysis of Test Hardware

Given the total fluid pressure drop, $\Delta P_{f,t}$ (from the top of the feeder tank

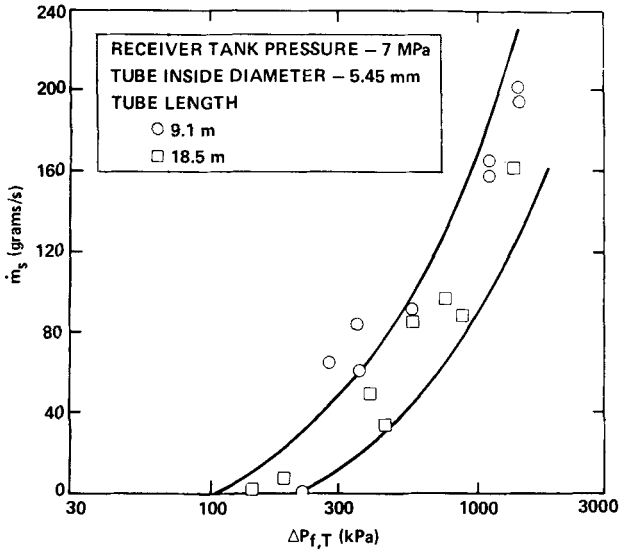

Figure 4. Solids flow rate vs. total system pressure drop through a 5.45-mm diameter tube (curves shown from Eq. 24 combined with Eqs. 11 and 25–28, parameters from Tables 1 and 2).

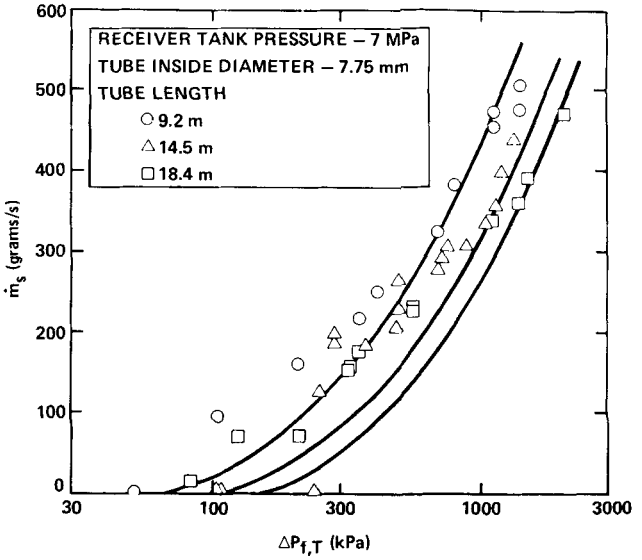

Figure 5. Solids flow rate vs. total system pressure drop through a 7.75-mm diameter tube (curves shown from Eq. 24 combined with Eqs. 11 and 25–28, parameters from Tables 1 and 2).

to the receiver tank) and the receiver tank fluid pressure, $P_{f,L}$, one can then predict the solids flow rate, $\dot{m}_s$, the fluid flow rate, $\dot{m}_f$, and the fluid pressure drop through the transport line, $\Delta P_{f,L}$, once the ball valve is opened. It is known that the solids mass flow rate for constant ϵ is given by:

$$\dot{m}_s = \frac{\pi D_t^2 (1-\epsilon)\rho_s v_{s,t}}{4} \tag{20}$$

Likewise, the transport fluid mass flow rate for constant ϵ and ρ_f is:

$$\dot{m}_f = \frac{\pi D_t^2 \epsilon \rho_f v_{f,t}}{4} \tag{21}$$

The total fluid pressure drop is defined as:

$$\Delta P_{f,T} = (P_{f,-\infty} - P_{f,L}) \tag{22}$$

and the transport line fluid pressure drop is:

$$\Delta P_{f,L} = (P_{f,o} - P_{f,L}) \tag{23}$$

Combining Eqs. 14, 15 and 19 with Eqs. 20 through 23 and reinvoking Assumptions L and M will show that the solids flow rate is predicted by the equation:

$$\dot{m}_s = \frac{\dot{m}_f (1-\epsilon)\rho_s}{\epsilon \rho_f} - \frac{\pi D_t (1-\epsilon)^2 \rho_s C_{WF} P_{f,L}}{\mu b} \tag{24}$$

In Eq. 24 the fluid flow rate is

$$\dot{m}_f = \frac{\pi \epsilon D_t^2 \rho_f (\sqrt{4c_1 c_3 + c_2^2} - c_2)}{8c_1} \tag{25}$$

where the three quadratic constants are given by:

$$c_1 = \frac{\rho_f}{2C_D^2} \tag{26}$$

$$c_2 = \frac{4L\mu\sqrt{b}}{D_t} \tag{27}$$

$$c_3 = \Delta P_{f,T} - \frac{4LC_{WF}(1-\epsilon)P_{f,L}}{D_t} \tag{28}$$

Finally, the fluid pressure drop in the transport line is given by:

$$\Delta P_{f,L} = \frac{4L}{D_t}\left[C_{WF}(1-\epsilon)P_{f,L} + \frac{4\mu\sqrt{b}\dot{m}_s}{\rho_s(1-\epsilon)\pi D_t^2}\right] \tag{29}$$

As seen in Eqs. 24 through 29 only the two friction coefficients, C_D and C_{WF}, remain to be determined before the solids and fluid flow rates can be predicted. Numerical values for these coefficients will be presented in the next section. A major characteristic of the solids and fluid flows is that they will stop anytime c_3 is less than or equal to zero. This is very important, since any time the total pressure drop between the feeder and receiver tanks is not sufficient to overcome the transport line friction resistance, there will be no solids and fluid flow.

RESULTS

Sixty-four dense-phase flow tests were conducted for this study in the facility shown in Figure 2 (Combs, 1982). Six different single transport line geometries were tested: a 5.45 mm inside diameter, D_t, transport tube with line lengths, L, of 9.1 and 18.5 m; a 7.75 mm transport tube with line lengths of 9.2, 14.5 and 18.4 m; and a 13.39 mm tube with a line length of 18.2 m. For all tests the receiver tank fluid pressure, $P_{f,L}$, was kept constant at 7 MPa while the total fluid pressure differential between the feeder and receiver tanks, $\Delta P_{f,T}$, was varied from 50 to 2,000 kPa.

Figures 4, 5, and 6 plot the results of this testing for the three tube diameters of 5.45, 7.75 and 13.39 mm, respectively. The solids flow rate is plotted against the total system pressure drop. As seen in these figures, the experimental data show that the solids flow rate decreases with decreasing pressure drop until a minimum pressure drop is reached below which no solids flow can be sustained.

The curves drawn through the data in Figures 4, 5 and 6 were calculated from Eq. 24 which uses Eqs. 11 and 25–28. The solids and fluid properties used in these equations are in Table 1. The

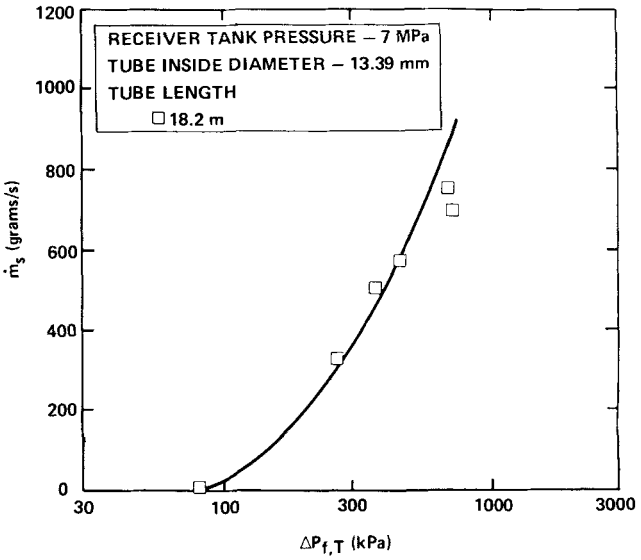

Figure 6. Solids flow rate vs. total system pressure drop through a 13.39-mm diameter tube (curve shown from Eq. 24 combined with Eqs. 11 and 25–28, parameters from Tables 1 and 2).

TABLE 2. DENSE-PHASE FEEDING MODEL FRICTION COEFFICIENTS AND STANDARD DEVIATIONS OF DATA AND CORRELATION

Friction Coefficients	
Feeder Tank Fluid Discharge, C_D	0.177
Tube Wall, C_{WF}	5.18×10^{-6}
Solids Flow Rate Standard Deviations (g/s)	
Experimental Data	161
Model Correlation	72

fluid mass density of the transport nitrogen gas was taken as the average density between the feeder and receiver tanks for each test condition. The two friction coefficients, C_D and C_{WF}, required for this system of modeling equations were determined by curve fitting Eqs. 11 and 24–28 to the experimental data using a nonlinear least-squares curve-fitting computer routine. The "best fit" parameters for these two coefficients are shown in Table 2 along with the standard deviations of the experimental data and model correlation.

Single fluid discharge coefficients can range from 0.60 for square-edged orifices to greater than 0.98 for well designed venturi flowmeters. The fluid discharge coefficient for dense-phase flow from a conical hopper is shown in Table 2 to be extremely low at 0.177. This low value may be the result of additional friction losses between the solids and converging tube wall; these losses are not present in single fluid flow. However, the low fluid discharge coefficient may also be the result of applying Assumptions I and O in the converging hopper analysis. Previous studies in the gravity flow of solids out of hoppers have shown that the solids will shear in the hopper's converging section with a resulting increase in this region of the void fraction, ϵ. It was expected for the loosely-packed coal beds prepared for testing in this study that variations in ϵ within the converging section of the feeder tank would be minimized. More effort in understanding the low numerical value obtained for the fluid discharge coefficient is surely required.

Assumptions I and O might also be responsible for the relative larger error between model and experiment seen for the 5.45 and 7.75 mm transport tubes (Figures 4 and 5) than with the larger 13.39 mm tube (Figure 6). The smaller feeder tank outlet openings will most likely produce a higher propensity within the bulk solids to shear as they pass through the converging section of the feeder.

The value for the coefficient of tube wall friction, C_{WF}, shown in Table 2 indicates that the ratio of the solids surface area fraction between the tube wall and bulk stream, α, is extremely small on the order of 10^{-5}. This can be seen from Eq. 16 with typical effective wall friction angles, δ_w, of 10 to 20 degrees. Actual experimental values of α at static conditions are not known for pulverized coal, but one would reasonably expect this number to be rather small.

The predicted transport fluid flow rate, from Eq. 25, was not compared against experimental data, since for these tests instrumentation malfunctions prevented the flow rate measurement of the nitrogen gas going to the feeder tank for pressurization. Without this flow, the experimental transport nitrogen flow rate cannot be obtained. However, earlier testing by Combs et al. (1980) had shown that the mass flow rate ratio between the solids and carrier gas in a high-pressure dense-phase coal feed system is approximately equal to

$$\frac{(1-\epsilon)\rho_s}{\epsilon\rho_f}.$$

This is the same result as predicted by Eq. 24, since the last term in this equation is essentially zero. Therefore, one could have reasonably expected the same type of fluid flow rate prediction for these tests as was obtained for the solids flow rate.

Due to problems encountered with the porous metal screen pressure tap located at the test line entrance (Figure 2), consistent experimental data for the gas-phase test line pressure drop was not obtained. Therefore, Eq. 29 was not compared with actual data. When the porous metal screen becomes plugged with micron-size particles, the response time of the pressure drop measuring system becomes quite long, at least much longer than the 2- to 4-minute test duration of each dense-phase flow data point obtained during this program.

ACKNOWLEDGMENTS

This work was funded by the U.S. Department of Energy under Contract Nos. DE-AC22-80PC30018 and DE-AC01-78ET10328. The experimental effort was conducted by R. F. Atkinson. A word of thanks needs to be given to L. P. Combs and D. R. Kahn for their support in the completion of this study.

NOTATION

$\vec{B}$ = fluid-solids drag body force vector, N/m^3
b = fluid-solids drag constant, m^{-2}
C_D = fluid discharge coefficient from a hopper or cone
C_{WF} = coefficient of tube wall friction
c_1 = first quadratic constant, kg/m^3
c_2 = second quadratic constant, kg/m^2·s
c_3 = third quadratic constant, Pa
D_p = particle diameter, m
D_t = inside diameter of transport tube, m
D_{31} = volume-diameter mean of the particle size number distribution, m
f_n = particle-size number distribution, number of particles in the diameter range dD_p about D_p, particles/m
$\vec{g}$ = gravitational acceleration vector, m/s^2
L = length of transport tube, m
$\dot{m}_f$ = fluid flow rate, kg/s
$\dot{m}_s$ = solids flow rate, kg/s
P_f = fluid pressure, Pa
$P_{f,L}$ = fluid pressure at the tube exit, Pa
$P_{f,o}$ = fluid pressure at the tube entrance, Pa
$P_{f,-\infty}$ = fluid pressure at the large end of a converging hopper or cone, Pa
P_s = solids pressure, Pa
$P_{s,o}$ = solids pressure at the tube entrance, Pa
r = radial distance, m
t = time, s
$\vec{v}_f$ = fluid velocity vector, m/s
$\vec{v}_s$ = solids velocity vector, m/s
v_f = fluid axial velocity, m/s
$v_{f,t}$ = fluid area averaged axial velocity in the tube, m/s
v_s = solids axial velocity, m/s
$v_{s,t}$ = solids area averaged axial velocity in the tube, m/s
z = axial distance, m

Greek Letters

α = ratio of the solids surface area fraction at the tube wall to the solids surface area fraction in the bulk
$\Delta P_{f,L}$ = fluid pressure drop through the transport line, Pa
$\Delta P_{f,T}$ = total fluid pressure drop from feeder tank to receiver tank, Pa
δ_w = effective angle of friction between the solids and tube wall, degrees
ϵ = void fraction
θ = half angle of a converging hopper or cone, degrees
κ = fluid bulk viscosity, kg/m·s
μ = fluid dynamic viscosity, kg/m·s
ρ_f = fluid density, kg/m^3
ρ_s = true solids density, kg/m^3
$\vec{\tau}_f$ = fluid stress tensor, Pa
$\vec{\tau}_s$ = solids stress tensor, Pa
$\tau_{s,rz}$ = solids shearing stress in the $r-z$ plane, Pa
ϕ = solids internal friction angle, degrees

LITERATURE CITED

Bird, R. B., W. E. Stewart, and E. N. Lightfoot, *Transport Phenomena*, Wiley, New York (1960).

Burge, H. L., R. W. Roberts, and E. V. Zettle, "Dense Phase Transport of Powdered Metals For a Tripropellant Rocket System," *Chem. Eng. Prog. Symp. Ser.*, **60**, No. 52, 30 (1964).

Combs, L. P., *Partial Liquefaction of Coal by Flash Hydropyrolysis, Phase IV Final Technical Report*, PETC-30018-6, Nat. Tech. Info. Service, Springfield, VA (1982).

Combs, L. P., S. K. Ubhayakar, L. S. Breese, D. R. Kahn, and W. T. Lee, *Coal Hydrogasification Process Development Second Annual Technical Progress Report Government Fiscal Year 1980, Vol. I: Coal Studies*, FE-3125-24, Nat. Tech. Info. Service, Springfield, VA (1980).

Friedman, J., *Development of a Single-Stage, Entrained-Flow, Short-Residence Time Hydrogasifier, Final Report*, FE-2518-24, Nat. Tech. Info. Service, Springfield, VA (1979).

Klinzing, G. E., *Gas-Solid Transport*, McGraw-Hill, New York (1981).

Kraus, M. N., *Pneumatic Conveying of Bulk Materials*, 2nd Ed., McGraw-Hill, New York (1980).

Mugele, R. A. and H. D. Evans, "Droplet Size Distribution in Sprays," *Ind. Eng. Chem.*, **43**, 1317 (1951).

Oberg, C. L., A. Y. Falk, G. A. Hood, and J. A. Gray, "Coal Liquefaction Under High-Mass Flux and Short-Residence Time Conditions," *Amer. Chem. Soc., Div. of Fuel Chem. Preprints*, **22**, No. 2, 185 (1977).

Oberg, C. L., A. Y. Falk, D. R. Kahn, and L. P. Combs, *Partial Liquefaction of Coal by Flash Hydropyrolysis, Final Technical Report*, FE-2044-52, Nat. Tech. Info. Service, Springfield, VA (1982).

Oberg, C. L. and G. A. Hood, *Dense-Phase Feeder Method*, U.S. Pat. 4,191,500 (1980).

Sandy, C. W., T. E. Daubert, and J. H. Jones, "Vertical Dense-Phase Gas-Solids Transport," *Chem. Eng. Prog. Symp. Ser.*, **66**, No. 105, 133 (1970).

Wen, C. Y., and W. S. O'Brien, "Pneumatic Conveying and Transporting," *Gas-Solids Handling in the Process Industries*, Marchello, J. M. and A. Gomezplata, Eds., Marcel Dekker, New York, 89 (1976).

Manuscript received July 14, 1982; revision received and accepted January 31, 1983.

Excess Second Virial Coefficients and Critical Temperatures: Acetone + Methyl Acetate

For the system acetone + methyl acetate measurements are reported of excess second virial coefficients (at 75 and 100°C) and critical temperatures for nine different compositions. The efficacy of the correlations due to Tsonopoulos and to Hayden and O'Connell are discussed and the former correlation (with one modification) is shown to give a better prediction of unlike interaction terms. The implication of the results for excess Gibbs Free Energy estimation is discussed.

P. J. McELROY, H. HASHIM, WONG LOKE TATT

Chemical Engineering Department
University of Canterbury
Christchurch, New Zealand

SCOPE

This study is part of a continuing program of measurement of unlike interaction second virial coefficients B_{ij} of a series of mixtures sufficiently diverse that procedures for the prediction of B_{ij} may be tested and the most successful methods identified. B_{ij} values are required in the determination of the PVT properties of gas mixtures at moderate pressure and in particular in the estimation of activity coefficients from vapor pressure studies. The enormous number of possible mixtures precludes measurement on all systems and so prediction is essential.

Most predictive techniques are variations on the principle of corresponding states and require "reduction" of temperature by a characteristic temperature, usually the pseudocritical temperature for unlike interaction, T^c_{12}. Preferably T^c_{12} is obtained from independent measurements such as the measured critical temperatures used here.

The particular system, acetone + methyl acetate, introduces two additional functional groups into the series studied. Also a recent liquid-vapor equilibrium investigation requiring B_{12} values exposed large differences in two of the most widely used predictive methods.

CONCLUSIONS AND SIGNIFICANCE

The unlike interaction second virial coefficient of the system, acetone + methyl acetate, has been measured and the inability of the correlations due to Tsonopoulos and to Hayden and O'Connell to accurately predict the results is demonstrated. Critical temperatures of this system have also been measured and employed to give an estimate of the unlike interaction pseudocritical temperature T^c_{12}. It is argued that a significant test of the predictive equations is only possible when T^c_{12} is not simply an adjustable fitting parameter but is independently estimated from measurements such as critical temperature. The fact that the Hayden-O'Connell correlation is superior in pure virial coefficient prediction but inferior in unlike interaction prediction suggests that the existing combining rules are inadequate.

INTRODUCTION

For mixing of two components, 1 and 2, in the gas phase, the pressure change, Δp, at constant volume and temperature is for moderate or low pressures simply related to the second virial coefficients (Knobler, 1967) B_{11},B_{22} (for the pure substances) and B_{12} (for unlike interaction).

$$RT\Delta p/p^2(1 + \Delta p/p)2x_1x_2 = B_{12} - \tfrac{1}{2}(B_{11} + B_{22}) = \epsilon \quad (1)$$

ϵ we will call the excess second virial coefficient.

One advantage of this method is that since ϵ may be measured more accurately than B_{ii} it is possible to estimate B_{12} with an error, δB, comparable to that in B_{11} and B_{22}. Estimation of B_{12} from the